Primary Oxidation Products of 5-Methylcytosine: Methyl Dynamics and Environmental Influences

André Krivokapić,*,† Kjell Tage Øhman,† William H. Nelson,‡ Eli O. Hole,† and Einar Sagstuen†

Department of Physics, University of Oslo, N-0316 Oslo, Norway, and Department of Physics and Astronomy, Georgia State University, Atlanta, Georgia 30303

Received: May 20, 2009; Revised Manuscript Received: July 15, 2009

The primary oxidation product in X-irradiated single crystals of 5-methylcytosine hemihydrate and 5-methylcytosine hydrochloride has been studied at 10 K, using electron paramagnetic resonance (EPR), electron−nuclear double resonance (ENDOR), and ENDOR-induced EPR (EIE) spectroscopies. The radical is characterized by large couplings to the methyl protons and appears to be deprotonated at N1 in both crystal systems. In the hydrochloride crystal the methyl group is completely frozen at 10 K, whereas in the hemihydrate crystal it undergoes tunneling rotation. For the hemihydrate crystal, four ENDOR lines associated with transitions within the A and E rotational states were followed in three planes of rotation. Large ENDOR shifts as measured by saturation of the high- and low-field parts of the EPR spectrum indicate that the rotation is rather slow. Sidebands due to mixing of A and E rotational states are expected for slow rotation and were observed in both the EPR and the EIE spectra. The ENDOR shifts and the sideband frequencies indicate a tunneling splitting between 40 and 60 MHz. Estimates of the barrier to rotation in both crystalline systems were calculated using cluster and single-molecule density functional theory methods, and the results are consistent with those obtained by analysis of the experimental results.

1. Introduction

Recently, methylated CpG sequences have been established as mutational hotspots in DNA, one reason of which being oxidation of 5-methylcytosine.[1] Four to five percent of the cytosines in DNA are 5-methylcytosine (m^5C, Chart 1 below).[2] m^5C has a lower ionization potential than cytosine[3] and may therefore better compete with guanine as a hole trap. Holes formed by ionizing radiation in the base regions of DNA may thus become trapped at m^5C. Once oxidized, the m^5C radical may irreversibly deprotonate at the methyl group and form a highly stable radical known as the 3αH radical[4] (Chart 2 below) with a lifetime sufficiently long to impair normal enzymatic activity which in many situations depends on demethylation of m^5C. To better understand the electronic properties of m^5C as a hole trap, and the mechanisms that form the stable end product, the structure of the initial electron-loss product of m^5C, which is stable only at low temperatures, needs to be determined.

Based on studies of the primary oxidation products in other cytosine derivatives[5,6] the one-electron oxidation product is expected to have a structure where a large part of the electron spin is coupled with the methyl protons in β-position. At low temperatures the methyl group is normally not able to rotate classically. However, the methyl protons may tunnel through the restricting potential barrier at a rate sufficiently high to give significant physical and spectroscopic effects. Understanding the electronic structure and the spectroscopic properties of the m^5C cation thus requires an understanding of the methyl group dynamics in the system.

CHART 1: 5-Methylcytosine, m^5C

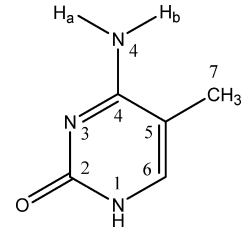

CHART 2: 3αH Radical

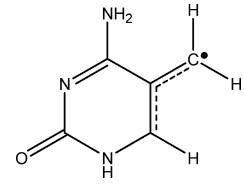

When the methyl group undergoes tunneling rotation in a threefold symmetric hindering barrier, the ground torsional-oscillator methyl group state is split into a singlet and a degenerate doublet with symmetries A and E, respectively, separated in energy by the tunneling splitting $h\nu_t$.[7] Further splitting arises when these states are combined with spin functions of appropriate symmetry. The electron−nuclear double resonance (ENDOR) spectra originating from this rotationally restricted spin system depend largely on the tunneling A−E splitting and provide a means to directly measure this splitting,[8−10] which is a sensitive function of the rotation barrier.[11] When the tunneling splitting is of similar magnitude as the hyperfine interaction, sidebands are expected to appear on each side of the electron paramagnetic resonance (EPR) spectrum.[12,13] These sidebands arise when the electron spin transition is accompanied

* To whom correspondence should be addressed. Tel.: +47 228 57687. Fax: +47 228 55671. E-mail: andre.krivokapic@fys.uio.no.
† University of Oslo.
‡ Georgia State University.

10.1021/jp904747j CCC: $40.75
Published on Web 08/10/2009

by a change of the methyl group rotational state and provide an additional way to measure the tunneling frequency.

In the present work, single crystals of 5-methylcytosine hemihydrate and 5-methylcytosine hydrochloride have been X-irradiated at 8−10 K and studied at this and higher temperatures using EPR, ENDOR, and ENDOR-induced EPR (EIE) spectroscopy in addition to single-molecule and cluster density functional theory (DFT) calculations at the B3LYP level. The electrostatic environment differs considerably in the two crystal lattices, and the experimental results indicate that for the primary oxidation product at low temperatures the methyl group undergoes hindered rotation by tunneling in the hemihydrate crystal while being completely frozen in the hydrochloride crystal.

The tunneling splitting obtained from both the ENDOR and the sideband spectra gives a barrier to methyl rotation in good agreement with that estimated from the DFT calculations.

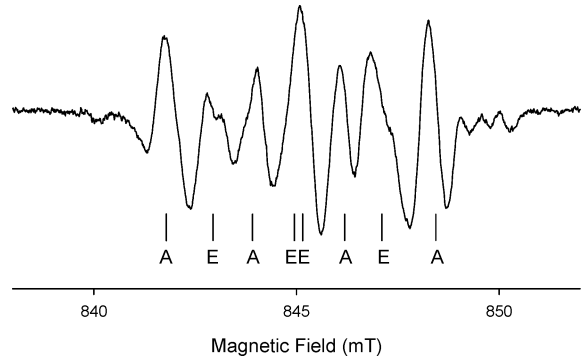

Figure 1. Second-derivative K-band EPR spectrum of a single crystal of 5-methylcytosine hemihydrate X-irradiated and measured at 10 K. The magnetic field was aligned 50° from *c* in the *a***c* plane. The stick diagram indicates the association with the methyl group rotational states.

2. Experimental Section

Single crystals of 5-methylcytosine hemihydrate and 5-methylcytosine hydrochloride (obtained from *NBS Biologicals* and *Sigma-Aldrich*, respectively) were grown by slow evaporation at 40−50 °C. Crystals of 5-methylcytosine hemihydrate are monoclinic with space group *C*2/*c* and eight asymmetric units in the unit cell (eight bases and four waters of crystallization).[14] The molecules are extensively connected by hydrogen bonds between neighboring molecules and through the water molecules; the amino protons are hydrogen bonded to N3 and O2 of neighboring bases, N1 is hydrogen bonded to water, and N3 is hydrogen bonded to N4 of a neighboring molecule.

Crystals of 5-methylcytosine hydrochloride are monoclinic with space group $P2_1/c$ and with four asymmetric units in the unit cell.[15] The molecules are protonated at N3, thus making the bases positively charged. In contrast to the hemihydrate crystal, the hydrochloride crystal structure shows little character of hydrogen bonding. The crystal structure is stabilized by electrostatic interactions between Cl^- ions and atoms of the bases and only one proper hydrogen bond between N3 and Cl^-.

The experimental procedures including K-band EPR, ENDOR, and EIE spectroscopies and computational techniques were as previously described.[16] The hydrochloride and hemihydrate crystals were X-irradiated to doses up to 60 and 100 kGy, respectively, at approximately 8−10 K (hereafter referred to as 10 K) and studied at this and higher temperatures. An orthogonal *a***bc* reference system was used for both crystals. The data for the hemihydrate crystals were collected by rotation around *b*, *c*, and a skewed axis located 90° from *c* and 30.5° from *a**. The hydrochloride data were collected by rotation around *a*, *b*, *c*, and a skewed axis located 67° from *c* and −3° from *a**.

DFT computations were performed using the quantum chemistry package *Gaussian 03* (G03), Revision D.02.[17] All calculations used the hybrid functional B3LYP and the split-valence triple-ζ basis set 6-311G(d,p), including one set of polarization functions to the hydrogens and to the heavy atoms. The default G03 optimization routines and convergence criteria were used for the optimizations. All single-point calculations were done with the scf convergence criteria scf = tight.

The methyl rotational barriers were calculated both for single molecules and for cluster systems by rotating the methyl group 120° around the C5−CH_3 axis in steps of 10°, with optimization carried out at each step. This was made by constraining the dihedral angle C6−C5−C7−H of one of the methyl protons during geometry optimization. This angle was subsequently altered as described. The difference between the maximum and minimum energy configurations of the 12-step iteration yields an estimate of the barrier to methyl rotation. For the single-molecule calculations, all other atomic coordinates were optimized at each step. The two different cluster systems used each consisted of a central molecule surrounded by several other molecules at positions provided by crystallographic data. The clusters included those molecules/Cl^- ions that were closest to the methyl group and to the amino group of the central molecule. The hemihydrate and the HCl cluster consisted of eight 5-methylcytosine molecules each, including one water and seven Cl^- ions, respectively. All atomic coordinates in the cluster were frozen during optimization except those of the methyl protons, the amino protons, and the C6−H proton, all belonging to the central molecule. All cluster calculations were performed on nonradical systems since for the clusters the unpaired spin did not become located solely on the radical molecule but delocalized over several of the molecules constituting the cluster. This is a technical problem sometimes observed in this type of calculations.[18]

3. Analyses and Results

3.1. 5-Methylcytosine Hemihydrate. Due to the presence of several radicals, the EPR spectra were not easily interpretable. However, the spectra seemed to be dominated by a seven- or eight-line pattern as shown in Figure 1, which is characteristic for radicals with a β-coupling to a methyl group ($C^{\bullet}-CH_3$) that undergoes tunneling rotation in a threefold barrier.[7] There are three radicals that are expected to have a large spin density on C5: the one-electron oxidation product (hereafter somewhat imprecisely called the cation), its N1 deprotonated successor, and the 5-yl H-addition radical.[19] The latter also has two large β-couplings to the methylene protons at C6 that give a characteristic broad EPR spectrum. At 10 K the EPR spectra showed little or no sign of lines associated with this 5-yl H-addition radical. Nor did the ENDOR or EIE spectra show lines attributable to the associated methylene protons. Instead the spectra are consistent with those for a cation or a nitrogen-deprotonated successor where only the methyl protons give large couplings.

Hindered methyl group rotation has been studied extensively by Clough and co-workers,[8−10,12,13,20] and some of their results relevant for the present study will briefly be repeated here. The methyl group is assumed to be in its ground torsional-oscillator state at very low temperatures.[8,21] As a result of tunneling rotation, this ground state is split into states with spatial

symmetries A and E that are separated in energy by the tunneling splitting $h\nu_t$. The exclusion principle requires that the A and E rotational states are combined with A and E nuclear spin states, respectively, leading to an EPR spectrum with eight lines where the two lines in the middle usually overlap. Transitions within these lowest rotational states may be described by the spin Hamiltonian

$$H/h = \nu_S S_z - \nu_n \sum_{j=1}^{3} I_{jz} + \sum_{j=1}^{3} \mathbf{S}\cdot\mathbf{T}_j\cdot\mathbf{I}_j - 2J \sum_{j>k=1}^{3} \mathbf{I}_j\cdot\mathbf{I}_k \quad (1)$$

The terms are, respectively, the electron Zeeman, the nuclear Zeeman, the hyperfine interactions, and the nuclear exchange interaction that gives rise to a splitting equivalent to the tunneling splitting $3J = \nu_t$. In this expression the nuclear dipole−dipole interaction between adjacent methyl protons has been omitted due to its small effect. Symmetrized eigenfunctions of the dominant terms in eq 1 then serve as a basis for perturbation expansion. For fast rotation ($\nu_t \gg T_{j,iso}$) the EPR transitions occur to first order at frequencies $\nu = \nu_S + (m/3)(T_{zz}^A + \lambda T_{zz}^E)$, where m is the z-component (defined by the magnetic field direction) of the total nuclear spin (from +3/2 to −3/2), T_{zz}^A and T_{zz}^E are the z-components of the A and E state coupling tensors $\mathbf{T}^A$ and $\mathbf{T}^E$, respectively, and λ is 0 and ±1 for the A and E states, respectively. Tensors $\mathbf{T}^A$ and $\mathbf{T}^E$ are nearly isotropic with similar magnitudes and are related to the methyl proton coupling tensors $\mathbf{T}_j$ as

$$\mathbf{T}^A = \mathbf{T}_1 + \mathbf{T}_2 + \mathbf{T}_3 \quad (2)$$

$$\mathbf{T}^E = 2\mathbf{T}_1 \cos(2\varphi) + 2\mathbf{T}_2 \cos(2\varphi - 2\pi/3) + 2\mathbf{T}_3 \cos(2\varphi + 2\pi/3) \quad (3)$$

where φ is the methyl group twist angle that locates one of the methyl protons on the circle through the three proton positions, being defined as ±90° when the proton lies in the nodal plane of the electron π-orbital. The two other protons are positioned at $\varphi \pm 120°$. The outermost EPR lines are thus separated by T_{zz}^A and the second outermost lines by $(T_{zz}^A + T_{zz}^E)/3$ and so on. Figure 2 shows an energy level diagram[9] illustrating the four ENDOR transitions of interest in the present report. To first order the high-frequency ENDOR transitions occur at $\nu_n + (1/6)(T_{zz}^A + \lambda T_{zz}^E)$. Second-order corrections alter the central pair of each quartet in the diagram which lead to a shift in ENDOR frequencies. With the magnetic field along a principal direction for $\mathbf{T}^A$, and disregarding terms with ν_S in the denominator, the new expressions for the high-frequency transitions in the A state ($m_S = -1/2$) become[9]

$$\nu_1 \approx \nu_{n1} + T_{zz}^A/6 + \frac{1}{36}|T_{zz}^{E'}|^2\left(\nu_t + \frac{1}{12}T_{zz}^E\right)^{-1} + \frac{1}{36}|T_{zz}^{E''}|^2\left(\nu_t - \frac{1}{12}T_{zz}^E\right)^{-1} \quad (m_I = -3/2 \leftrightarrow -1/2) \quad (4)$$

$$\nu_2 \approx \nu_{n2} + T_{zz}^A/6 + \frac{1}{36}(|T_{zz}^{E'}|^2 - |T_{zz}^{E''}|^2)\left\{\left(\nu_t - \frac{1}{12}T_{zz}^E\right)^{-1} - \left(\nu_t + \frac{1}{12}T_{zz}^E\right)^{-1}\right\} \quad (m_I = -1/2 \leftrightarrow 1/2) \quad (5)$$

$$\nu_3 \approx \nu_{n3} + T_{zz}^A/6 - \frac{1}{36}|T_{zz}^{E'}|^2\left(\nu_t - \frac{1}{12}T_{zz}^E\right)^{-1} - \frac{1}{36}|T_{zz}^{E''}|^2\left(\nu_t + \frac{1}{12}T_{zz}^E\right)^{-1} \quad (m_I = 1/2 \leftrightarrow 3/2) \quad (6)$$

where the tensors $\mathbf{T}^{E'}$ and $\mathbf{T}^{E''}$ are related to $\mathbf{T}^E$ as

$$\mathbf{T}^{E'} = \sqrt{\frac{1}{2}}\mathbf{T}^E \cos\varphi \quad \text{and} \quad i\mathbf{T}^{E'} = \sqrt{\frac{1}{2}}\mathbf{T}^E \sin\varphi \quad (7)$$

For very high barriers giving slow rotation ($\nu_t \ll T_{j,iso}$), the tunneling splitting is treated as a perturbation in eq 1.[20] The EPR spectrum is then basically the same as that for a static methyl group, but the ENDOR lines become shifted. To first order the ENDOR line shift resulting from locking the magnetic field to the high-field part and to the low-field part of the EPR spectrum is $\nu^h - \nu^l - (\nu_n^h - \nu_n^l) = -(4/3)\nu_t$. One important consequence is that this shift is negative in this latter case while it is positive in the fast tunneling situation. By measuring the value of this shift the tunneling frequency ν_t can be determined.

When the tunneling splitting is of similar magnitude as the hyperfine splitting, sidebands are expected to appear in the EPR spectrum.[12] These are forbidden EPR transitions between A and E $m_I = \pm 1/2$ states that become allowed due to mixing of these states through the hyperfine interaction. Their intensities relative to unity for the main EPR lines depend on the twist angle φ and tunneling splitting ν_t approximately as

$$((T_{zz}^E)^2/18\nu_t^2)\cos^2 3\varphi \quad \text{for} \quad \lambda = -1 \quad \text{and} \quad ((T_{zz}^E)^2/18\nu_t^2)\sin^2 3\varphi \quad \text{for} \quad \lambda = 1 \quad (8a)$$

and the frequencies at which these lines occur are to first order, respectively

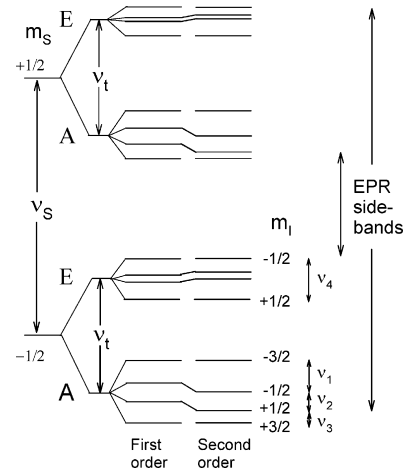

Figure 2. Schematic energy level diagram, illustrating the high-frequency ENDOR lines and second-order shifts that occur as a result of tunneling rotation. Also shown are two EPR sideband transitions that are observed.

$$\nu_S \pm \nu_t \pm (T_{zz}^A/6 - T_{zz}^E/12) \quad \text{and} \quad \nu_S \pm \nu_t \pm (T_{zz}^A/6 + T_{zz}^E/12) \quad (8b)$$

Figure 3 shows ENDOR spectra obtained by saturation of the corresponding EPR lines shown at the bottom part in Figure 4 marked with numbers. (The center EPR line did not give ENDOR signals.) The spectra were recorded at 10 K with the magnetic field parallel to a^*. At this orientation the magnetic field is close to being in the molecular plane where nitrogen couplings are small, thus increasing the spectral resolution. ENDOR lines $\nu_1-\nu_3$ are assigned to transitions within the methyl group A state (see Figure 2) and line ν_4 to a transition in the E state. Also shown in Figure 4 are EIE spectra from ENDOR lines $\nu_1-\nu_5$. The main features of the EPR spectrum may be explained by the stick diagram shown below in Figure 4. At this orientation all the lines are split by about 0.5 mT, which corresponds to an ENDOR line at about 43 MHz and is indicated as ν_5 in Figure 3. This ENDOR line is assigned to an N−H α-coupling (see below).

The outermost lines on each side of the EPR spectrum are believed to be sidebands. It is seen that ENDOR lines ν_1 and ν_3 are observed when the high-field and low-field parts of the EPR spectrum are saturated, corresponding to $A_{mI=-3/2}$ and $A_{mI=+3/2}$ transitions, respectively. Line ν_2 is observed from saturation of both of the EPR $A_{mI=\pm1/2}$ transitions and from the low-field sideband. ν_4 is observed from saturation of the high- and low-field E lines as well as from the high-field sideband.

These relationships are confirmed by the EIE spectra showing the EPR lines that are connected to each of the ENDOR transitions. ENDOR line ν_5 was observable from most EPR lines, and the EIE spectrum from this line, although only partially resolved, appears to reproduce the entire EPR spectrum. From these observations it is concluded that lines $\nu_1-\nu_4$ are indeed the ENDOR transitions indicated in Figure 2 and that the large (positive) ENDOR shift originates from hindered rotation. The association of the low-field and high-field sidebands to ν_2 and ν_4, respectively, is as expected from the diagram in Figure 2.

The line ν_5 was only observed in two planes of rotation, but based on its anisotropy and previous ENDOR studies of the cytosine cation,[5] it is believed to belong to an N4−H_a α-coupling. This is supported by the presence of another line (ν_6) in one plane of rotation with anisotropy and coupling strength corresponding to the other amino proton (N4−H_b). Estimates of the principal values for the α-couplings to the two amino protons are given in Table 1, indicating ∼0.10 π-spin density at N4 with a Q^N-value of −80 MHz in the McConnell relation.[22] The weaker coupling to H_b compared with that to H_a is attributed to the proximity of H_b to a large spin density at C5.[4,5] Single-molecule DFT calculations indicate a spin density at N1 of about 0.22 for the pristine cation and about 0.30 for the N1 deprotonated species. Since no ENDOR line associated with an N1−H coupling was observed, it is suggested that the radical species in question is the N1-deprotonated one-electron oxidation product as shown in Chart 3, designated **R1**(hemi).

Figure 5 shows the angular variations in three planes of rotation for ENDOR lines $\nu_1-\nu_4$. The anisotropy of the lines was determined by doing a standard calculation for hyperfine proton coupling tensors with the results given in Table 1. All tensors $\mathbf{T}_{\nu1}-\mathbf{T}_{\nu4}$ have axial symmetry as expected for β-couplings.

As is illustrated in Figure 6a, compared with the crystallographic data[14] the eigenvectors for the maximum principal values of $\mathbf{T}_{\nu1}$, $\mathbf{T}_{\nu3}$, and $\mathbf{T}_{\nu4}$ (with the set of signs in Table 1) appear to be roughly parallel to the directions from C5 to the three methyl protons while the corresponding eigenvector for $\mathbf{T}_{\nu2}$ is approximately parallel to the C5−CH_3 direction. The latter is expected since ν_2 deviates least from A symmetry. A better correlation is obtained (Figure 6b) by rotating the methyl group around the C5−CH_3 axis by 12° and rotating this axis around an axis normal to the molecular plane, also by 12°. Provided that these eigenvectors reflect the methyl proton positions, the deviation from the crystallographic directions is probably a result of the tunneling rotation or it may suggest that the radical as a whole becomes twisted or tilted upon formation, possibly as an effect of deprotonation.

The ENDOR lines thus exhibit an anisotropy as expected from both a static and a rotating methyl group. One reason for this

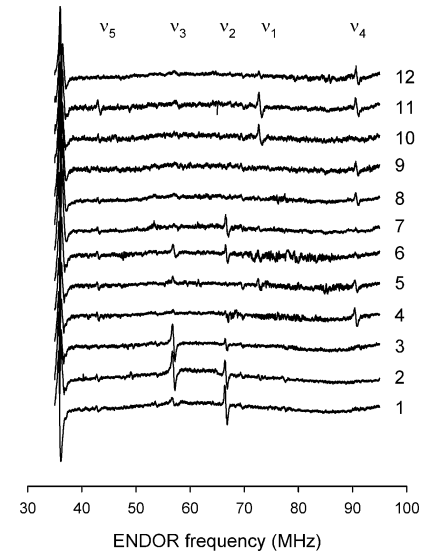

Figure 3. ENDOR spectra of 5-methylcytosine hemihydrate with the magnetic field aligned along a^*, X-irradiated and observed at 10 K. The numbers indicate the corresponding EPR lines in Figure 4.

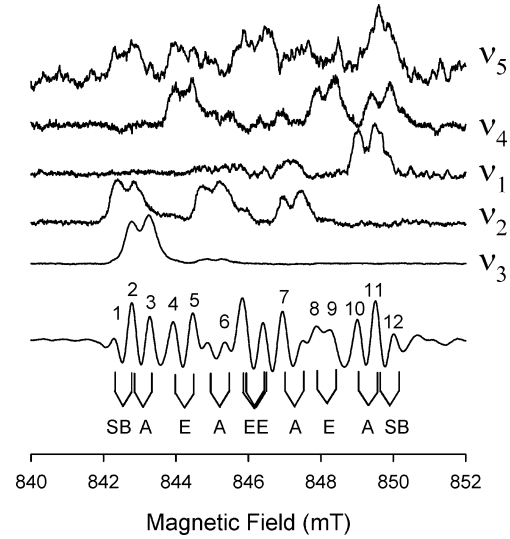

Figure 4. Second-derivative K-band EPR (bottom) and EIE spectra of a single crystal of 5-methylcytosine hemihydrate X-irradiated at 10 K, with the magnetic field aligned with a^*. The EPR spectrum and the EIE spectrum for ν_5 were measured at 10 K, while the other spectra were obtained at 30 K for better signal-to-noise ratio. The stick diagram indicates the association with the methyl group A and E states. The splitting of the lines is caused by an N4−H_a α-coupling. The outermost lines (marked SB) are assumedly sidebands.

TABLE 1: Hyperfine Coupling Tensors[a] for the Oxidation Product (Radical R1(hemi)) Resonances Observed in Single Crystals of 5-Methylcytosine Hemihydrate at 10 K

			eigenvectors		
tensor	isotropic value (MHz)	principal value (MHz)	*a**	*b*	*c*
		74.5 (1)	0.914 (1)	0.405 (20)	0.008 (30)
$^{b}\mathbf{T}_{\nu 1}$	70.5 (1)	68.6 (1)	0.345 (2)	−0.770 (43)	−0.537 (69)
		68.4 (1)	0.211 (2)	−0.494 (75)	0.844 (48)
		61.6 (1)	0.993 (1)	0.083 (3)	0.084 (2)
$^{b}\mathbf{T}_{\nu 2}$	58.1 (1)	57.0 (1)	0.026 (2)	0.537 (14)	−0.843 (9)
		55.8 (1)	0.115 (3)	−0.839 (9)	−0.531 (14)
		44.2 (1)	0.764 (3)	0.087 (7)	0.639 (16)
$^{b}\mathbf{T}_{\nu 3}$	40.6 (1)	39.3 (1)	0.617 (6)	−0.388 (26)	−0.685 (11)
		38.2 (1)	0.188 (4)	0.918 (9)	−0.350 (21)
		111.1 (1)	0.869 (1)	0.478 (2)	−0.130 (4)
$^{b}\mathbf{T}_{\nu 4}$	105.9 (1)	104.0 (1)	0.494 (2)	−0.853 (2)	0.167 (8)
		102.5 (1)	0.031 (1)	0.210 (9)	0.977 (2)
		−15			
$\mathbf{T}_{\nu 5}$ (N4−H_a)	−8.3	−9	estimated from two data sets		
		−1			
		−11			
$\mathbf{T}_{\nu 6}$ (N4−H_b)	−6.7	−7	estimated from one data set		
		−2			
		184.8 (3)	0.993 (1)	0.083 (3)	0.084 (2)
$^{c}\mathbf{T}^{A}$	174.4 (3)	171.0 (3)	0.026 (2)	0.537 (14)	−0.843 (9)
		167.4 (3)	0.115 (3)	−0.839 (9)	−0.531 (14)
		155.8 (3)	0.617 (2)	0.761 (7)	−0.202 (3)
$^{c}\mathbf{T}^{E}$	145.2 (3)	142.3 (3)	0.495 (2)	−0.574 (4)	−0.652 (8)
		137.4 (3)	0.613 (4)	−0.302 (7)	0.730 (6)
C5−CH_3 direction			0.935	−0.126	0.333

[a] Numbers in parentheses represent standard deviation in the last digit(s). [b] Obtained from standard calculation for hyperfine couplings. [c] Obtained from first-order expressions for ENDOR lines ν_2 and ν_4.

CHART 3: Radical R1(hemi)

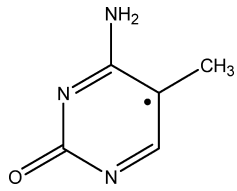

seeming contradiction might be that the tunneling rotation is rather slow (see below) and in a region where the ENDOR transitions show characteristics from both of these two states. The possibility of having two sets of methyl groups, one static and one rotating fast,[20,23] is rejected for two reasons. First, the isotropic values of $\mathbf{T}_{\nu 1}$, $\mathbf{T}_{\nu 3}$, and $\mathbf{T}_{\nu 4}$ are not all together consistent with the expression for isotropic β-couplings, $a_{iso}^{\beta} = \rho^{\pi}(B_0 + B_2 \cos^2 \theta)$,[24] where ρ^{π} is the spin density at C5, B_0 and B_2 are constants depending on spin polarization and hyperconjugation, respectively, and $\theta = \varphi$, $\varphi \pm 120°$. Second, the isotropic value of $\mathbf{T}_{\nu 3}$ is far too large for a dihedral angle θ close to 90° (Figure 6).

ENDOR frequencies $\nu_1-\nu_4$ closely resemble those found for hindered methyl group rotation of the thymine H-addition radical reported by Box et al.,[25] although in that work the data were insufficient to yield the anisotropic properties.

Tensors $\mathbf{T}^{A}$ and $\mathbf{T}^{E}$ in Table 1 were obtained using the first-order expressions $\nu_2 = \nu_{n2} + (1/6)T_{zz}^{A}$ and $\nu_4 = \nu_{n4} + (1/6)(T_{zz}^{A} + T_{zz}^{E})$. According to eq 5, this leads to an overestimation of $\mathbf{T}^{A}$, and consequently to an underestimation of $\mathbf{T}^{E}$. An indication of the magnitude of this overestimation can be found from the width of the EPR spectra, which represents the total coupling from the methyl protons and thus $\mathbf{T}^{A}$. In Figure 4 the magnetic field is parallel to a^*, which, according to Table 1, is approximately the principal axis for the maximum principal value of $\mathbf{T}^{A}$. The EPR lines $m_I = \pm 3/2$ are separated by ca. 174 MHz, while ENDOR line ν_2 indicates a width of almost 185 MHz. There is scarce information in the literature on the tensor $\mathbf{T}^{E}$,[9,21] and because of the issue discussed above it is difficult to interpret the anisotropy of $\mathbf{T}^{E}$ in Table 1.

According to the crystallographic data, the methyl group twist angle φ is approximately 30° and the information from the eigenvectors does not indicate a large deviation from this value. Equation 5 then becomes $\nu_2 = \nu_{n2} + T_{zz}^{A}/6 + [(T_{zz}^{E})^2/144][(\nu_t - T_{zz}^{E}/12)^{-1} - (\nu_t + T_{zz}^{E}/12)^{-1}]$. The value of T_{zz}^{E} is found from the EPR spectrum in Figure 4 to be ca. 143 MHz, and with $T_{zz}^{A} =$ 174 MHz the tunneling frequency becomes about 45 MHz.

Turning to the ENDOR shift, we find from eqs 4−7 with $\varphi = 30°$ that $\nu_1 - \nu_3 - (\nu_{n1} - \nu_{n3}) = \nu_t(T_{zz}^{E})^2/\{36\,[\nu_t^2 - (T_{zz}^{E})^2/144]\}$, which becomes ca. 15.7 MHz at the orientation in Figure 4. $T_{zz}^{E} \approx 143$ MHz then gives a tunneling frequency $\nu_t \approx 40$ MHz.

According to eq 8a, with $\varphi = 30°$ only the outer pair of each sideband quartet, centered around ν_S, should be present. Why only the outermost member of these pairs was observed in the EIE spectra is not clear. With the above values for T_{zz}^{A} and T_{zz}^{E} and using eq 8b (for the outermost sideband lines), the tunneling frequency is found to be ca. 60 MHz. Exact expressions for the sideband frequencies based on a simplified Hamiltonian with only isotropic couplings to the methyl protons have previously been given by Mottley et al.[13] Solving the secular equation with matrix elements given in that paper, using $\varphi = 30°$, one finds the sidebands frequencies to be $\nu = \nu_S + (3/4)Am \pm \{[((1/2)\nu_t - (1/8)Am)^2 + (1/8)A^2m^2]^{1/2} + [((1/2)\nu_t + (1/8)Am)^2 + (1/8)A^2m^2]^{1/2}\}$, where $m = \pm 1/2$ is the nuclear spin and $A/2$ is the average isotropic methyl proton coupling. This expression gives for the sidebands in Figure 4, with $A = (2/3)T_{zz}^{A} = 116$ MHz, a tunneling frequency $\nu_t \approx 40$ MHz, in agreement with the value from the ENDOR data.

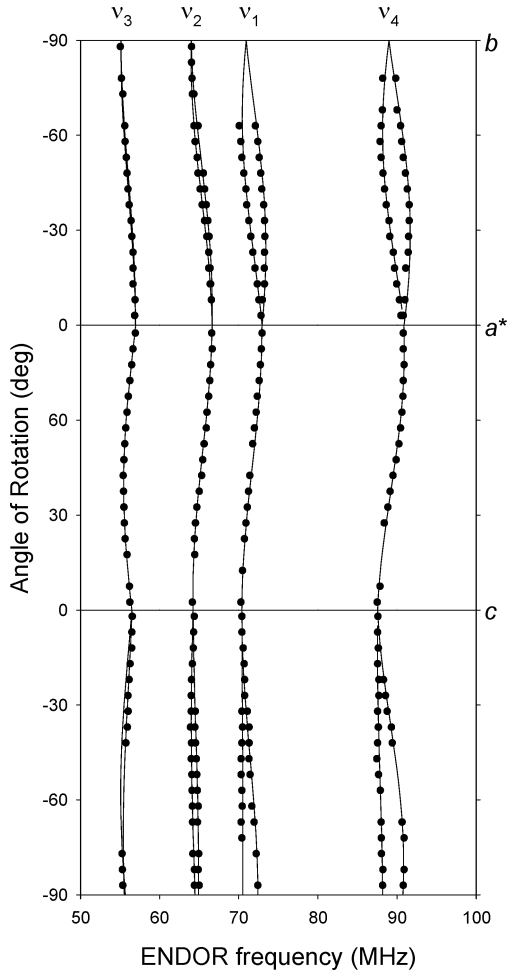

Figure 5. Angular variation of K-band ENDOR lines $\nu_1-\nu_4$ in three planes of rotation. The bottom plane is a skew plane. The solid lines are theoretical values calculated from the coupling tensors in Table 1.

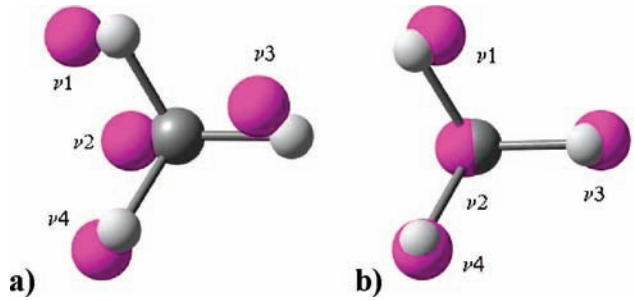

Figure 6. (a) Position for the methyl group (pink spheres) as indicated by the maximum principal value eigenvectors for $\mathbf{T}_{\nu 1}-\mathbf{T}_{\nu 4}$ compared with the methyl group position from crystallographic data (white/gray spheres) viewed along the CH_3-C5 direction. The molecular plane coincides with the horizontal plane in these figures. (b) Similar to (a), except for rigid coordinate rotations of the methyl group as described in the text.

With $\varphi = 30°$ and $\nu_t = 40-60$ MHz in eq 8a, the sidebands should have an intensity ratio of 0.3−0.7 relative to the main lines. The ratio of these lines in Figure 4 appears to be in that region. The sidebands were unresolved at several magnetic field orientations, as in Figure 1, most probably due to significant spectral broadening from nitrogen interactions, but they appeared consistently in the EIE spectra from ENDOR lines ν_2 and ν_4.

It is concluded that the tunneling frequency is between 40 and 60 MHz. Based on a relationship between the tunneling

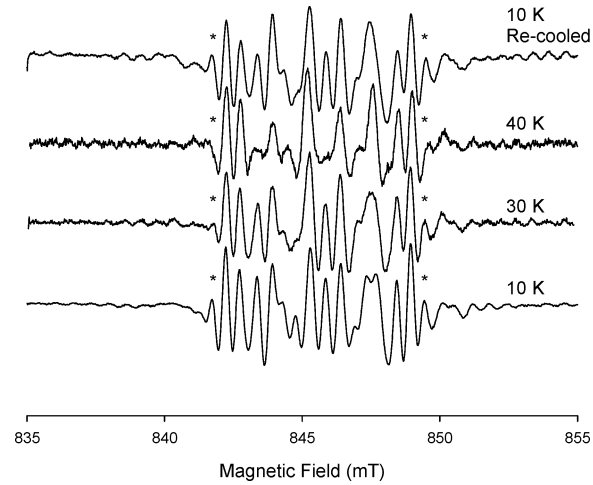

Figure 7. Second-derivative K-band EPR spectra of 5-methylcytosine hemihydrate with the magnetic field along a^*, X-irradiated at 10 K and warmed to the temperatures indicated. The asterisk indicates the outer sideband EPR lines. The spectra are normalized with respect to lines from other radicals that are believed to remain stable.

frequency and the barrier to rotation[11] presented graphically by Freed,[7] $\nu_t = 40-60$ MHz corresponds to a barrier of about 1.6−1.7 kcal/mol. The barrier for single molecules was estimated by DFT calculations by rotating the methyl group 120° in steps of 10° with otherwise full geometry optimization carried out at each step. The barrier obtained was 2.5 kcal/mol for a nonradical and 1.6 kcal/mol for radical **R1**(hemi), indicating that oxidation significantly lowers the barrier. The direct influence on the barrier from the surroundings was investigated by comparing the barrier obtained for a molecule (nonradical) in a cluster, as described in section 2, to the barrier obtained for a single molecule using the cluster geometries. These calculations gave barriers of 2.6 kcal/mol for the cluster and 2.9 kcal/mol for the single molecule with cluster geometry. This suggests that the intermolecular interactions in this crystal lattice do not increase the rotational barrier.

The relatively high rotational barrier suggests that the torsional oscillation is low, which should make the isotropic values of $\mathbf{T}^E$ and $\mathbf{T}^A$ nearly equal. The ratio of these values can be expressed as $T^E_{iso}/T^A_{iso} = (1-\delta)/(1+2B_0/B_2)$,[10] where $\delta = 2\langle(\varphi_j - \langle\varphi_j\rangle)^2\rangle$ is a measure of zero-point torsional oscillation and B_0 and B_2 are the constants in the Heller−McConnell relation for β-couplings.[24] The values in Table 1 give a ratio of 0.83. By comparing with what has been found in other systems, a ratio >0.94 should be expected.[10] The smaller ratio is most probably primarily due to that $\mathbf{T}^A$ in Table 1 is overestimated and $\mathbf{T}^E$ is underestimated. An additional possibility is that B_0 in this system is larger (approximately a few MHz) than B_0 in the former systems, although DFT calculations indicate a B_0 value close to zero.

Upon warming to 40 K, the EPR spectrum changed in two respects as shown in Figure 7. First, at 30 K the sideband EPR lines (marked with *) grew weaker and almost disappeared at 40 K. Second, the lines in the central part broadened and decreased compared to the outer lines. (The other prominent lines in the center-right part of the spectrum at 40 K mostly belong to another radical species, the 3αH radical[4] in Chart 2.) These changes might indicate a methyl motional averaging process that involves the $m_I = \pm 1/2$ lines and for which the outer $m_I = \pm 3/2$ lines remain unaffected. This temperature behavior also suggests that classical rotation, which mainly affects the E lines and at high temperatures gives the 1:3:3:1

TABLE 2: Hyperfine Coupling Tensors[a] for the Oxidation Product (Radical R2(HCl)) Resonances Observed in Single Crystals of 5-Methylcytosine Hydrochloride at 10 K

tensor	isotropic value (MHz)	principal value (MHz)	eigenvectors		
			*a**	*b*	*c*
		83.9 (1)	0.732 (1)	0.678 (1)	−0.066 (3)
$\mathbf{T}_{va}$	78.4 (1)	76.2 (1)	0.672 (1)	−0.734 (1)	−0.092 (3)
		75.0 (1)	0.111 (1)	−0.022 (5)	0.994 (1)
		81.1 (1)	0.406 (2)	0.580 (17)	0.706 (4)
$\mathbf{T}_{vb}$	75.9 (1)	73.8 (1)	0.219 (1)	−0.812 (2)	0.541 (16)
		72.9 (1)	0.887 (1)	−0.066 (9)	−0.457 (10)
C5−CH_3 direction			0.492	0.802	0.338

[a] Numbers in parentheses represent standard deviation in the last digit(s).

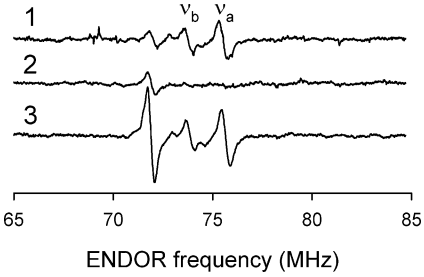

Figure 8. K-band ENDOR spectra from a single crystal of 5-methylcytosine hydrochloride, X-irradiated and observed at 10 K with the magnetic field along *b*. The numbers designate the field positions in Figure 9 at which the ENDOR spectra were acquired.

quartet,[8] is not significant at 40 K. Instead the motional averaging could be due to transitions between $m_I = \pm 1/2$ A and E states at different torsional vibrational levels, which broaden the $m_I = \pm 1/2$ A lines as well.[26] When recooling the crystal from 40 to 10 K, the 10 K main spectral features returned, including the sideband lines, consistent with such a dynamic process. ENDOR lines $\nu_1-\nu_4$ were present at 30 K and disappeared completely at 50 K, whereas no ENDOR line attributable to classical rotation of the methyl group appeared. Above 50 K, especially at 80 K, the resonance lines due to radical **R1**(hemi) started decaying, as evidenced by the outer main EPR lines disappearing and not reappearing by recooling to 10 K. Apparently, the radical decays before onset of rapid classical rotation.

3.2. 5-Methylcytosine Hydrochloride. EPR spectra from crystals of 5-methylcytosine hydrochloride X-irradiated at 10 K were dominated by lines from radicals other than the one-electron oxidation product, the most prominent being due to the 3αH radical. Only two ENDOR lines could be assigned to the (deprotonated) one-electron oxidation product, and the corresponding hyperfine coupling tensors are given in Table 2. Figure 8 shows these ENDOR lines (ν_a and ν_b, the line at 72 MHz is due to the 3αH radical) measured at 10 K with the magnetic field parallel to *b*, where the magnetic field positions are indicated in Figure 9. At this orientation the magnetic field is about 9° from the base plane, thus reducing nitrogen couplings.

Both tensors have similar principal values and exhibit axial symmetry, as expected for β-proton couplings. The crystallographic data[15] indicate that the methyl group twist angle φ is slightly less than 30°. The eigenvectors of the maximum principal values for tensors ν_a and ν_b deviate 3.5° and 4.0°, respectively, from the crystallographic directions from C5 to the two out-of-plane methyl protons. The coupling from the third proton is thus expected to be very small, and possibly too close

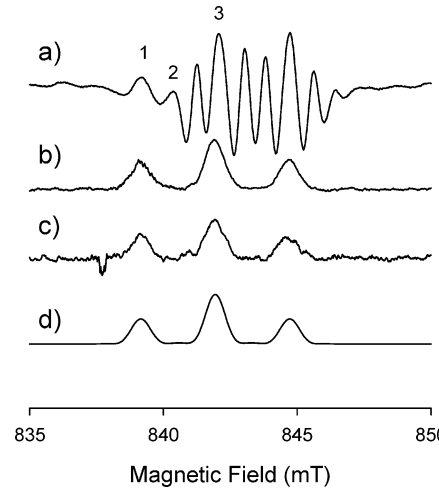

Figure 9. K-band EPR and EIE spectra from a single crystal of 5-methylcytosine hydrochloride, X-irradiated and observed at 10 K with the magnetic field along *b*. (a) Second-derivative EPR spectrum. (b) and (c) EIE spectra from ENDOR lines ν_a and ν_b, respectively. (d) Simulated absorption EPR spectrum based primarily on tensors $\mathbf{T}_{va}$ and $\mathbf{T}_{vb}$ in Table 2 (see text for details).

CHART 4: Radical R2(HCl)

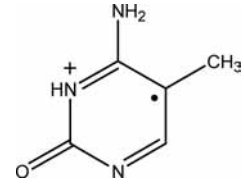

to the free-proton line to be generally detectable. ENDOR lines corresponding to a coupling of 4−6 MHz which gave the same EIE spectra as those in Figure 9 were however observed at some orientations.

As for the hemihydrate crystal, DFT calculations on N3-protonated m^5C indicate that the spin density at N1 is about 0.22 and 0.30 for the pristine cation and the N1-deprotonated species, respectively. An N1−H α-coupling is expected to have its maximum value at the orientation in Figure 9 and should give rise to a clearly observable splitting in the EIE spectra. Since the spectra do not show sign of such a splitting, it is concluded that the radical in question also in this crystalline system is the N1-deprotonated one-electron oxidation product, radical **R2**(HCl), as depicted in Chart 4.

The EIE spectra recorded from lines ν_a and ν_b were considerably broadened and unresolved at orientations where the magnetic field was closer to the ring normal, indicating considerable spin density at nitrogen atoms. The simulated EIE spectrum in Figure 9 is obtained by using the tensors in Table 2 and hyperfine coupling tensors for the amino protons and nitrogen coupling tensors corresponding to ca. 20−30% spin at N1 and about 10−15% at N4. At this orientation these latter couplings contribute only to the line width, however.

ENDOR from the low-field and the high-field EPR lines did not give rise to a detectable ENDOR shift beyond experimental uncertainty. The difference $\nu_a^h - \nu_a^l - (\nu_{na}^h - \nu_{na}^l)$ was close to zero (∼±0.01 MHz). This indicates that the methyl group is basically completely frozen and that there is a large barrier to rotation in this system. The barrier was estimated from DFT calculations in the same manner as described above for the hemihydrate crystal. The results for optimized single molecules were 2.1 kcal/mol for the nonradical and 1.2 kcal/mol for the N1-deprotonated cation (radical **R2**(HCl)). The influence from

the surrounding Cl^- ions was investigated by using the cluster (and the procedure) described in section 2. This gave a barrier of 3.7 kcal/mol for the central molecule (nonradical) in the cluster. Using the same geometries for a single molecule gave a barrier of 2.5 kcal/mol. The calculations thus indicate a substantial increase of the barrier due to the surrounding Cl^- ions.

Upon warming from 10 K to room temperature, ENDOR lines ν_a and ν_b disappeared at 110 K and the EPR lines at the positions of the EIE spectrum in Figure 9 decreased in intensity from 100 K. During this heat treatment the crystal was recooled from 200 to 10 K, which resulted in both the ENDOR lines and the main spectral features of the EPR spectrum reappearing. When recooling from room temperature to 10 K, neither the ENDOR lines nor the EPR spectral features reappeared. This demonstrates that radical **R2**(HCl) decays completely between 200 and 295 K and suggests that thermally activated rotation takes place somewhere at or above 110 K. No new ENDOR line which could be ascribed to tunneling or classical rotation for the **R2**(HCl) radical was observed, however.

4. Concluding Remarks

In both crystals the cation seems to have deprotonated at N1, indicating a predisposition for the m^5C cation to deprotonate at this site. However, DFT equilibrium energy calculations suggest that proton transfer to the hydrogen-bonded neighbors (H_2O and Cl^-) is not energetically favorable in either of the two crystals. Thus the proton may become trapped at other sites, possibly by additional proton transfer steps.

The **R2**(HCl) radical was far more stable than the corresponding radical **R1**(hemi), and apparently no transformation into other radical species upon warming occurred in either crystal. One of the reasons for the difference in thermal stability might be the lack of hydrogen bonding in the HCl crystal. This could reduce the electronic coupling strength between electron transfer donor and acceptor and thus reduce the recombination rate.[27] The extensive hydrogen-bonding network in the hemihydrate crystal may also facilitate recombination through a proton-coupled electron transfer mechanism,[28] similar to what has been observed in crystals of cytosine monohydrate.[29]

According to the DFT calculations, the barrier to methyl rotation in the hemihydrate crystal is mainly intramolecular. The amino proton H_b is probably the main contributor to the barrier due to its proximity to the methyl group. In the HCl crystals, however, the electrostatic interaction from the Cl^- ions appears to have as much effect on the barrier as do the intramolecular interactions. Thus, to identify the N1-deprotonated m^5C cation in more complex systems, information about the ionic surroundings should be useful when interpreting EPR and ENDOR spectra.

After X-irradiation of 5-methylcytosine hemihydrate crystals at room temperature, the 3αH radical is the dominant radical observed.[30] From the present work, the low-temperature (deprotonated) cation is apparently not the precursor for the room-temperature 3αH radical. Other low-temperature radical species, as well as the mechanistic pathways for understanding the room temperature results, are the subject of forthcoming publications.

Acknowledgment. The Norwegian Metacenter for Computational Science (NOTUR) is acknowledged for grants of computer time.

References and Notes

(1) Chen, J. X.; Zheng, Y.; West, M.; Tang, M. S. *Cancer Res.* **1998**, *58*, 2070.
(2) Ehrlich, M. *Oncogene* **2002**, *21*, 5400.
(3) Close, D. M. *J. Phys. Chem. B* **2003**, *107*, 864.
(4) Krivokapić, A.; Hole, E. O.; Sagstuen, E. *Radiat. Res.* **2003**, *160*, 340.
(5) Sagstuen, E.; Hole, E. O.; Nelson, W. H.; Close, D. *J. Phys. Chem.* **1992**, *96*, 8269.
(6) Hole, E. O.; Nelson, W. H.; Sagstuen, E.; Close, D. M. *Radiat. Res.* **1998**, *149*, 109.
(7) Freed, J. H. *J. Chem. Phys.* **1965**, *43*, 1710.
(8) Clough, S.; Poldy, F. *J. Chem. Phys.* **1969**, *51*, 2076.
(9) Clough, S.; Hill, J.; Poldy, F. *J. Phys. C: Solid State Phys.* **1972**, *5*, 518.
(10) Clough, S.; Poldy, F. *J. Phys. C: Solid State Phys.* **1973**, *6*, 1953.
(11) Hecht, K. T.; Dennison, D. M. *J. Chem. Phys.* **1957**, *26*, 31.
(12) Clough, S.; Hill, J.; Poldy, F. *J. Phys. C: Solid State Phys.* **1972**, *5*, 1739.
(13) Mottley, C.; Kispert, L. D.; Clough, S. *J. Chem. Phys.* **1975**, *63*, 4405.
(14) Grainger, C. T.; Bailey, D. *Acta Crystallogr.* **1981**, *37*, 2157.
(15) Padmaja, N.; Ramakumar, S.; Viswamitra, M. A. *Acta Crystallogr.* **1987**, *43*, 2157.
(16) Nelson, W. H.; Hole, E. O.; Sagstuen, E.; Close, D. M. *Int. J. Radiat. Biol.* **1988**, *54*, 963.
(17) Frisch, M. J.; Trucks, G. W.; Schlegel, H. B.; Scuseria, G. E.; Robb, M. A.; Cheeseman, J. R.; Montgomery, J. A., Jr.; Vreven, T.; Kudin, K. N.; Burant, J. C.; Millam, J. M.; Iyengar, S. S.; Tomasi, J.; Barone, V.; Mennucci, B.; Cossi, M.; Scalmani, G.; Rega, N.; Petersson, G. A.; Nakatsuji, H.; Hada, M.; Ehara, M.; Toyota, K.; Fukuda, R.; Hasegawa, J.; Ishida, M.; Nakajima, T.; Honda, Y.; Kitao, O.; Nakai, H.; Klene, M.; Li, X.; Knox, J. E.; Hratchian, H. P.; Cross, J. B.; Bakken, V.; Adamo, C.; Jaramillo, J.; Gomperts, R.; Stratmann, R. E.; Yazyev, O.; Austin, A. J.; Cammi, R.; Pomelli, C.; Ochterski, J. W.; Ayala, P. Y.; Morokuma, K.; Voth, G. A.; Salvador, P.; Dannenberg, J. J.; Zakrzewski, V. G.; Dapprich, S.; Daniels, A. D.; Strain, M. C.; Farkas, O.; Malick, D. K.; Rabuck, A. D.; Raghavachari, K.; Foresman, J. B.; Ortiz, J. V.; Cui, Q.; Baboul, A. G.; Clifford, S.; Cioslowski, J.; Stefanov, B. B.; Liu, G.; Liashenko, A.; Piskorz, P.; Komaromi, I.; Martin, R. L.; Fox, D. J.; Keith, T.; Al-Laham, M. A.; Peng, C. Y.; Nanayakkara, A.; Challacombe, M.; Gill, P. M. W.; Johnson, B.; Chen, W.; Wong, M. W.; Gonzalez, C.; Pople, J. A. *Gaussian 03*, revision D.02; Gaussian, Inc.: Wallingford, CT, 2004.
(18) Ohman, K. T.; Sagstuen, E. *J. Phys. Chem. A* **2008**, *112*, 4284.
(19) Bernhard, W. A. *Adv. Radiat. Biol.* **1981**, *9*, 199.
(20) Clough, S.; Hill, J. R.; Punkkinen, M. *J. Phys. C: Solid State Phys.* **1974**, *7*, 3779.
(21) Bonon, F.; Brustolon, M.; Maniero, A. L.; Segre, U. *Chem. Phys.* **1992**, *161*, 257.
(22) Nelson, W. H.; Gill, C. *Mol. Phys.* **1978**, *36*, 1779.
(23) Wells, J. W.; Box, H. C. *J. Chem. Phys.* **1967**, *46*, 2935.
(24) Heller, C.; McConnell, H. M. *J. Chem. Phys.* **1960**, *32*, 1535.
(25) Box, H. C.; Budzinski, E. E.; Potter, W. R. *J. Chem. Phys.* **1974**, *61*, 1136.
(26) Clough, S.; Starr, M.; McMillan, N. D. *Phys. Rev. Lett.* **1970**, *25*, 839.
(27) Bixon, M.; Jortner, J. *Adv. Chem. Phys.* **1999**, *106*, 35.
(28) Cukier, R. I.; Nocera, D. G. *Annu. Rev. Phys. Chem.* **1998**, *49*, 337.
(29) Krivokapić, A.; Herak, J. N.; Sagstuen, E. *J. Phys. Chem. A* **2008**, *112*, 3597.
(30) Hüttermann, J.; Ward, J. F.; Myers, L. S., Jr. *Int. J. Radiat. Phys. Chem.* **1971**, *3*, 117.

JP904747J